NANO LETTERS

Letter

pubs.acs.org/NanoLett

Plasmon Nanomechanical Coupling for Nanoscale Transduction

Rutger Thijssen,*[,†] Ewold Verhagen,[†,‡] Tobias J. Kippenberg,[‡] and Albert Polman[†]

[†]Center for Nanophotonics, FOM Institute AMOLF, Science Park 104, 1098XG Amsterdam, The Netherlands

[‡]École Polytechnique Fédérale de Lausanne (EPFL), Lausanne, Switzerland

ABSTRACT: We demonstrate plasmon-mechanical coupling in a metalized nanomechanical oscillator. A coupled surface plasmon is excited in the 25 nm wide gap between two metalized silicon nitride beams. The strong plasmonic dispersion allows the nanomechanical beams' thermal motion at a frequency of 4.4 MHz to be efficiently transduced to the optical transmission, with a measured displacement spectral density of 1.11×10^{-13} m/Hz$^{1/2}$. When exciting the second-order plasmonic mode at λ = 780 nm we observe optical-power-induced frequency shifts of the mechanical oscillator. Our results show that novel functionality of plasmonic nanostructures can be achieved through coupling to engineered nanoscale mechanical oscillators.

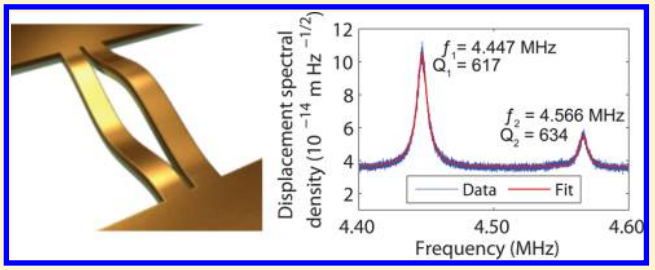

KEYWORDS: *Plasmonics, optomechanics, resonator, Brownian motion*

Nanomechanical oscillators are attracting a large interest for the sensitive detection of forces, displacements, or masses or as elements offering novel optical functionality. A variety of methods to transduce nanomechanical motion have been developed: electrically,[1−5] cavity-enhanced,[6,7] and by using photonic crstals[8] or optical waveguides.[9,10] While optical transduction schemes offer high bandwidth and low noise—enabling nanomechanical motion to be measured at the standard quantum limit,[11,12] and can display a variety of radiation pressure-related effects,[13,14] they are typically limited by the diffraction limit. Here, we take advantage of the strong confinement of the optical near fields in plasmonic systems and realize a nanoscale cavity[15] with deep subwavelength confinement in two dimensions, to transduce[16] the thermal motion of two nanomechanical oscillators composed of two planar Si_3N_4 nanobeams[17] to an optical far field.

The natural confinement offered by the evanescent field of surface plasmon polaritons is widely used for the sensing of refractive index changes[18] and could likewise be employed to detect the position of nanoscopic bodies.[19] While nanoscale optomechanical structures have enabled optomechanical coupling strengths as high as $G \equiv (\partial\omega_c/\partial x) < 500$ GHz/nm,[14,20] where ω_c is the mechanical oscillator dependent optical cavity resonance frequency, the strong coupling between plasmonic modes,[21−23] as shown in this work, allows structures to be realized whose optomechanical coupling in principle exceed 2 THz/nm. In conjunction with the high plasmon resonance frequency, the latter provides the basis for high frequency transduction of displacements,[24] leading in turn to high frequency transduction of, for example, mass changes[25] or weak forces,[26] as well as potentially allowing measurement of plasmonic mediated forces. This architecture is sensitive to a broad range of wavelengths throughout the optical spectrum and can be engineered for enhanced sensitivity at given wavelengths. Moreover, this method relies on straightforward free-space coupling, allowing future integration and parallelization, in particular far-field readout of massive arrays of nanomechanical oscillators. Finally, our approach can be extended to localized plasmonic nanoparticles and thereby be used as a local probe of nanomechanical vibration with a three-dimensional subwavelength scale.

Figure 1A shows a cartoon of a generic plasmonic nanomechanical geometry, showing the main parameters and typical length scales. The actual experimental structure is composed of two parallel freestanding doubly clamped 50-nm-thick Si_3N_4 bars, coated on one side with a 120-nm-thick Au layer using thermal evaporation. The nanomechanical Si_3N_4 bars are suspended in a Si_3N_4 membrane, that itself is suspended in a Si(100) wafer (Norcada, Canada) (Figure 1B). The nanobeams are fabricated by focused ion beam milling, using a 35 keV Ga^+ beam (current 9.7 pA) to mill three parallel 20-μm-long slits through the Au-coated membrane. The two outer slits are 100 nm wide, while the central gap width is varied between 15 and 120 nm for different structures. A top-view scanning electron microscopy image of the structure is shown in Figure 1C. Due to strong residual stress in the silicon nitride layer the membrane on the outer side of both nanobeams bends away, increasing the size of the two outer gaps, while the central gap keeps its width as fabricated. Figure 1F shows a magnified view of a structure with a 25-nm central gap size.

The relative mechanical motion of the nanobeams is probed by measuring the transmission of a laser beam that is incident normal to the sample, with its focus centered on the middle slit.

Received: April 25, 2013
Revised: June 5, 2013
Published: June 9, 2013

   dx.doi.org/10.1021/nl4015028 | *Nano Lett.* 2013, 13, 3293−3297

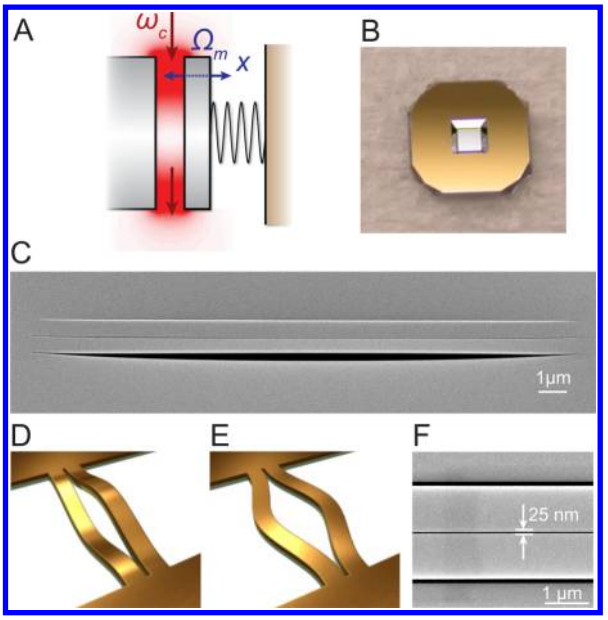

Figure 1. Plasmonic nanomechanical transducer geometry. (A) Illustration of a generic plasmonic nanomechanical resonator. (B) Photograph of the silicon nitride membrane used as a base for fabrication. (C) Scanning electron micrograph (incident angle 52°) of the double bridge structure after fabrication. The two-bridge structure is freestanding and lifted above the surrounding membrane due to mechanical stress in the latter. (D) Cartoon of the antisymmetric out-of-plane mechanical mode of the double bridge structure. (E) Cartoon of the antisymmetric in-plane mechanical mode of the double bridge structure. (F) Scanning electron micrograph (incident angle 0°) of the center part of the double bridge, showing the 25-nm-wide central gap. The Au layer is visible as the grainy structure on top.

The laser excitation generates metal−insulator−metal (MIM) plasmons that are confined within the 25-nm-gap suspended by the Au layers. Figure 2A shows the calculated plasmon dispersion relation[27] for a semi-infinite gold-vacuum-gold MIM waveguide (see inset) for gap widths ranging from 120 to 10 nm. As the width of the insulator gap region is reduced, the plasmonic coupling between the two metal interfaces becomes stronger, increasing the wave vector and the effective index of the plasmonic MIM mode[28] and thus increasing nanomechanical wavelength shifts.

Figure 2B shows a 2D finite-difference-time-domain simulation (Lumerical Solutions) of the transmission through the 120-nm-long experimental waveguide (see inset). Several characteristic resonant features are seen in the transmission spectrum. In the range 700−800 nm, a resonant Fabry-Pérot mode is observed that results from the reflection of the MIM plasmon at the upper and lower dielectric discontinuities defining the MIM cavity. As the gap width is reduced, the plasmon wave vector increases, and the resonance redshifts. The inset in Figure 2C shows the field distribution at 750 nm for a 20 nm gap width, corresponding to the first-order (n = 1) Fabry-Pérot resonance that occurs when the cavity length is equal to one-half of a plasmon wavelength, taking into account the phase jump at the interfaces.[29] Note that the strong resonance shift with gap width in this plasmonic MIM cavity geometry is due to the strong sensitivity to dispersive plasmonic effects rather than being linearly linked to a mirror displacement as is the case in conventional Fabry-Pérot cavities. Figure 2C shows the position and relative shift of the n = 1 Fabry-Pérot resonance frequency for different gap widths. From the data shown in Figure 2B, we extract the peak positions of the n = 1 resonance and calculate G, the optical frequency shift per unit displacement, with units of [Hz]/[m]. This can be used to

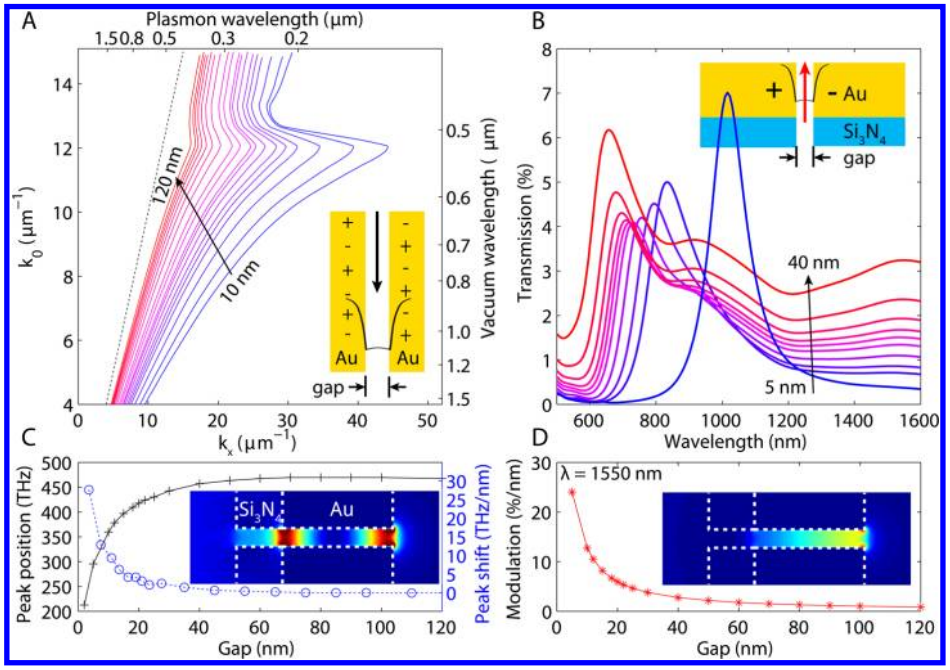

Figure 2. Dispersion of metal−insulator−metal plasmons. (A) Calculated dispersion relation for a gold-air-gold metal−insulator−metal (MIM) waveguide, shown schematically in the inset, with the mode profile indicated in black. The width of the air gap ranges from 10 nm (blue) to 120 nm (red). The light line is indicated by the dashed black line. (B) Simulated (FDTD) transmission through a 120 nm long MIM cavity, as shown in inset, with gap widths from 17 to 59 nm. (C) Calculated resonance frequency as a function of gap width for the n = 1 Fabry-Pérot mode (black) and differential peak shift (blue) at each gap width. (D) Calculated modulation of transmission for the n = 0 mode at λ = 1550 nm. The insets in C and D show the electric field intensity $|E|^2$ of the two modes for a gap width of 20 nm.

dx.doi.org/10.1021/nl4015028 | *Nano Lett.* 2013, 13, 3293−3297

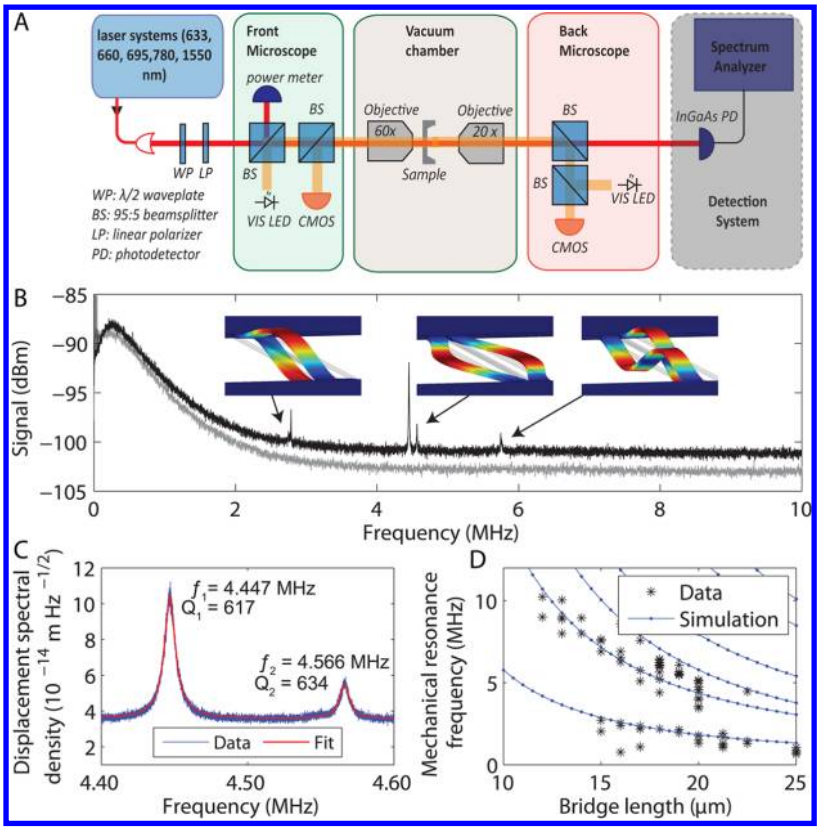

Figure 3. Nanomechanical frequency spectra of plasmonic nanoresonators measured at 1550 nm. (A) Schematic of the experimental setup. Various lasers have been used in the experiment, with wavelengths between 633 and 1550 nm. The input power and polarization is controlled by using a half-wave plate followed by a linear polarizer, with the wave plate mounted in a motor-driven rotation stage. The input power is monitored using a beamsplitter and a calibrated power meter. A microscope is used to align the sample on the incoupling microscope. The sample and in- and outcoupling objectives are placed on motor-driven stages in a custom built vacuum chamber evacuated to 10^{-3} mbar using a turbomolecular pump. A second microscope is used to align the outcoupling objective. The transmitted light is then sent to a fiber-coupled amplified photodiode. The AC output is monitored on a spectrum analyzer, while the DC output is monitored on an oscilloscope. (B) Black line: Mechanical spectrum measured using a spectrum analyzer. Four mechanical resonances are visible, at ν = 2.8, 4.5, 4.6, and 5.75 MHz. The broad peak centered at 250 kHz is attributed to laser noise. The insets show FEM simulations of the associated mechanical modes. Gray line: Mechanical spectrum of a reference sample, consisting of a double beam structure in low-stress (200 MPa) silicon nitride without gold, offset by −3 dBm. No mechanical resonances are observed. (C) Higher-resolution-bandwidth measurement of the mechanical resonances around 4.5 MHz. The data very well fit a double-Lorentzian line profile superimposed on a constant background representing the detector noise floor. The low- and high-frequency degenerate resonances have quality factors Q = 617 and Q = 634, respectively. The signal amplitude corresponds to a RMS mechanical amplitude x_{rms} = 10.4 pm, in agreement with theory, demonstrating the high displacement sensitivity of the plasmonic nanocavity. (D) Resonance frequencies (*) for bridges with lengths ranging between 12 and 25 μm, compared to FEM simulations (blue lines).

derive many optomechanical interaction parameters. For instance, the radiation pressure per photon is $\hbar G$. For gaps smaller than 40 nm, the simulated optomechanical coupling constant is larger than 2 THz/nm, which is larger than has been shown in any optomechanical system to date. At longer wavelengths, the n = 0 plasmonic mode is excited, which modulates the transmitted intensity as a function of gap width, as shown in Figure 2D.

To investigate the transduction of the nanomechanical motion to the optical signal, we use the experimental setup shown schematically in Figure 3A. A narrowband (short-term line width <100 kHz) λ = 1550 nm CW laser is focused through the center slit of a double beam structure, with TM polarization, exciting the MIM plasmon. The transmitted light is collected using a 200 MHz bandwidth InGaAs photodiode. The photodiode signal is converted to the frequency domain using a spectrum analyzer. The sample chamber is pumped down to below 10^{-3} mbar to minimize viscous drag from the ambient air on the nanobeams.

Figure 3B shows the frequency spectrum of the signal transduced by the plasmonic nanocavity. Four mechanical resonances are clearly observed, at ν = 2.75, 4.4, 4.6, and 5.8 MHz. To corroborate the mechanical nature of these resonances, we fabricated a series of bridges with lengths between 12 and 25 μm. For all these bridges, we measured spectra similar to the one shown in Figure 3B and extracted the mechanical resonance frequencies, which are plotted in Figure 3D. These measured eigenfrequencies show good agreement to finite-element-method (COMSOL) simulations of the mechanical eigenfrequencies of the bridges, assuming a reasonable value for the stress in the Si_3N_4 membrane ($\sigma \approx$ 700 MPa). This simulation also allows us to identify the nature of the mechanical eigenmodes at the different resonant frequencies, with corresponding FEM simulations inset in Figure 3B. We find that the modes near 2 MHz correspond to out-of-plane oscillation of the beams (sketched in Figure 1D), while modes in the 4−5 MHz spectral range are due to in-plane oscillation of the beams (Figure 1E). The 5.8 MHz resonance matches the second order out-of-plane mode. The insets in Figure 3B show

dx.doi.org/10.1021/nl4015028 | Nano Lett. 2013, 13, 3293−3297

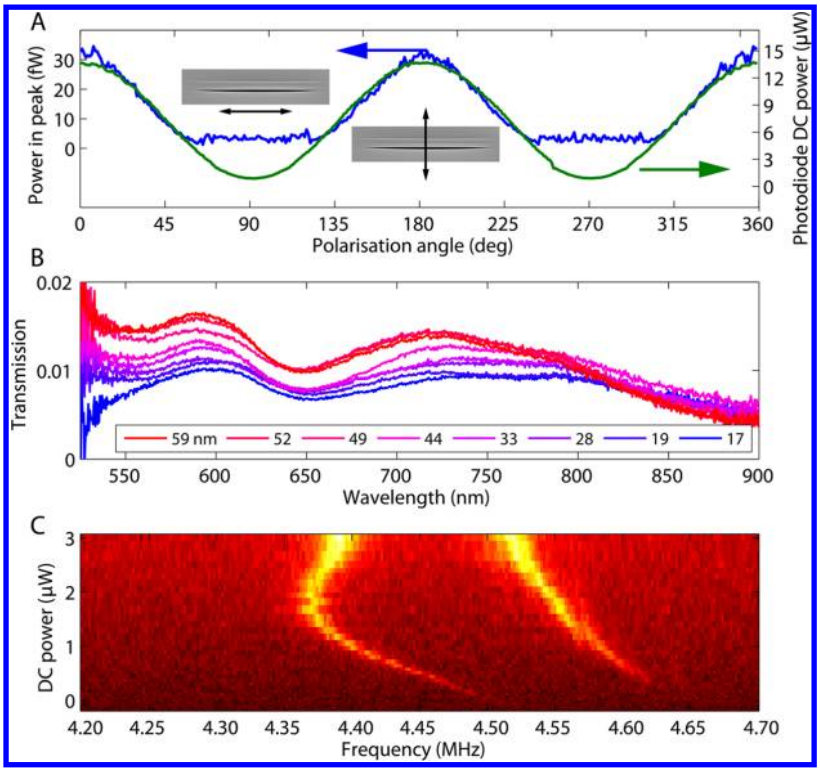

Figure 4. Polarization dependence, white light spectra, and power-dependent frequency shifts of mechanical motion in a plasmonic nanoresonator. (A) Polarization dependence at 780 nm (0 deg = TM polarization). Blue curve: Measured amplitude of mechanical resonance peak at ν = 4.5 MHz. Green curve: total optical power transmitted through the structure. For this measurement, the linear polarizer was removed, leaving the input power constant while rotating the polarization. The signal amplitude at ν = 4.5 MHz follows the transmitted power curve, showing the plasmonic behavior of the central slit. For TE polarizations (at 90 and 270°), the signal strength is determined by the detector noise floor. The arrows in the inset SEM micrographs show the E-field polarization relative to the double bridge structure. (B) Experimental white light spectroscopy of transmission through double bridge structures. Two resonances are visible: the tail of the n = 0 localized surface plasmon mode peaking at λ = 1500 nm (inset 2D) and the n = 1 Fabry-Pérot mode at λ = 750 nm (inset 2C). The inset shows the gap widths used, as measured with a scanning electron microscope. These widths have a relative measurement uncertainty of ±3%. (C) Power-dependent mechanical spectra measured at λ = 780 nm. The lower frequency mode first decreases in frequency and increases in frequency for higher powers.

FEM simulations of the associated modes. Figure 3B also shows a reference measurement taken on a Si_3N_4 bridge structure without gold film. Manufacturing narrow slits in the σ = 700 MPa membranes without gold coatings was unsuccessful: the beams collapsed onto each other during milling, due to the high stress in the membrane. However, this structure was successfully milled in a lower-stress membrane, with $\sigma \approx$ 200 MPa. From FEM simulations for this geometry, comparable to those in Figure 3D, the lowest order out-of-plane and in-plane modes would be expected at 4.41 and 18.5 MHz, respectively. No mechanical modes are observed, clearly demonstrating that detection of mechanical motion observed in the metallic bridges is due to MIM plasmons in the narrow metal gaps.

Figure 3C shows a more detailed view of the resonant modes at ν = 4.447 and 4.566 MHz. The observation of the doublet resonant modes is attributed to the lifting of the degeneracy of the double-bridge resonant modes by small differences in bridge sizes resulting from slight differences in the ion milling parameters. Lorentzian line shapes are fitted through the resonances, adding a constant background due to photodetector noise. Good agreement with the data is observed, with quality factors of Q = 617 and 634, respectively, for the two modes. These values being close again testifies to the degenerate nature of the two resonant modes. The mechanical quality factor is limited in these structures by the large amount of gold on the beams. By depositing gold only in the optically probed region of the beams, the quality factor could likely be improved.[30]

From the Lorentzian line fits the energy stored in each mechanical mode is determined. Dividing by the known DC electrical power output from detection photodiode a signal modulation depth of 5.2×10^{-4} is found. Using the simulated intensity modulation of 0.05/nm at λ = 1550 nm for a gap width of 20 nm (Figure 2C), this corresponds to a RMS amplitude of the mechanical mode of δ_{rms} = 10.4 pm. From the equipartition theorem we find $\delta_{rms} = (k_B T/m_{eff}\nu^2)^{1/2}$ = 15 pm, with an effective mass m_{eff} = 42.5 pg, in good agreement with the measurement given the uncertainties in material parameters. These data demonstrate the high displacement sensitivity of the plasmonic nanocavities. We have also compared these data to the modulation expected from a knife-edge modulation. In the naive approach, taking only the geometric width change into account without any resonant effects, the transmitted intensity scales with the gap width, leading to a modulation of $\delta x/x_0$. For the measured transduction at λ = 1550 nm, these values are close to each other. However, near the resonance at 780 nm, plasmonic transduction offers higher sensitivity. This can be understood from Figure 2B, as the transduction benefits especially from strong plasmonic mode dispersion with the laser tuned to the side of the resonant peak.

To further verify that the optomechanical spectra shown in Figure 3 are due to cavity plasmonic resonances, we studied the

dx.doi.org/10.1021/nl4015028 | Nano Lett. 2013, 13, 3293−3297

dependence on incident polarization, while keeping the incident power constant. Figure 4A shows the optomechanical resonance peak intensity as a function of polarization angle. A sinusoidal trend is observed with maxima and minima for TM and TE polarization, respectively, directly proving the plasmonic nature of the coupling mechanism. For TE polarization, the mechanical peak is no longer visible above the detector noise background.

We have also systematically varied the gas pressure in the measurement chamber: the signal gradually reduces and the line width increases for increasing pressures; the signal disappears above approximately 1 mbar, showing that the signal is indeed mechanical in origin.

Figure 4B shows optical transmission data for double-beam slits in the red and near-infrared spectral range, probing the n = 1 plasmonic localized mode. Light from a fiber-coupled halogen lamp was focused on the central slit using a confocal transmission microscope. The light is incident on the Si_3N_4 side of the membrane (see inset Figure 2B) to optimize impedance matching from the free-space incident beam to the MIM plasmon mode. The spot size diameter was about 1.5 μm. The light transmitted through the slit was spectrally analyzed using a fiber-coupled grating spectrometer equipped with a silicon deep-depletion CCD detector. A clear resonance is observed near 700−750 nm, varying with gap width, as also seen in the calculation shown in Figure 2B. The dip between 600 and 650 nm is attributed to light propagating around the outer edges of the beams, which were not included in the FDTD simulations shown in Figure 2B.

Finally, we performed power-dependent measurements of the plasmonic nanocavity resonance spectrum using an external-cavity diode laser operating at λ = 780 nm. When exciting the system at λ = 780 nm, the main mechanical mode at 4.4 MHz first redshifts for increasing power and then blue-shifts, as shown in Figure 4C. The origin of these nonlinear effects at high power will be the subject of further study.

In conclusion, we demonstrated a plasmonic optomechanical resonator with high displacement sensitivity. Light is coupled to plasmonic localized Fabry-Pérot resonances that show large amplitude modulation with small mechanical displacements of the cavity, with an optomechanical coupling constant larger than 2 THz/nm. We detect the fundamental cavity mechanical mode ν = 4.447 MHz, with a quality factor Q = 617 and determine an RMS amplitude of the mechanical mode as small as δ_{rms} = 10.4 pm, with a displacement sensitivity given by 3.58 × 10^{-14} m/$Hz^{1/2}$. Nonlinear effects are observed at high laser power and might pave the way to further control over nanomechanical motion. These plasmonic nanocavities provide a rapid, effective, and ultrasensitive readout method of nanoscale mechanical motion that could be of use in both fundamental and applied studies, in which nanomechanical systems act as transducers, sensors, or active elements.

AUTHOR INFORMATION

Notes

The authors declare no competing financial interest.

ACKNOWLEDGMENTS

This work is part of the research programme of the Foundation for Fundamental Research on Matter (FOM), which is financially supported by The Netherlands Organisation for Scientific Research (NWO). This work is supported by the European Research Council. E.V. acknowledges support from the Marie Curie IEF grant USOM. T.J.K. acknowledges support from the NCCR of Quantum Engineering and from DARPA ORCHID.

REFERENCES

(1) Cleland, A. N.; Roukes, M. L. *Nature (London)* **1998**, *392*, 160.
(2) Lahaye, M. D.; Suh, J.; Echternach, P. M.; Schwab, K. C.; Roukes, M. L. *Nature (London)* **2009**, *459*, 960.
(3) Ekinci, K. L.; Roukes, M. L. *Rev. Sci. Instrum.* **2005**, *76*, 061101.
(4) Faust, T.; Krenn, P.; Manus, S.; Kotthaus, J. P.; Weig, E. M. *Nat. Commun.* **2012**, *3*, 728.
(5) Hanay, M.; Kelber, S.; Naik, A.; Chi, D.; Hentz, S.; Bullard, E.; Colinet, E.; Duraffourg, L.; Roukes, M. *Nat. Nanotechnol.* **2012**, *7*, 602.
(6) Teufel, J. D.; Donner, T.; Castellanos-Beltran, M. A.; Harlow, J. W.; Lehnert, K. W. *Nat. Nanotechnol.* **2009**, *4*, 820.
(7) Kippenberg, T. J.; Rokhsari, H.; Carmon, T.; Scherer, A.; Vahala, K. J. *Phys. Rev. Lett.* **2005**, *95*, 033901.
(8) Eichenfield, M.; Camacho, R.; Chan, J.; Vahala, K. J.; Painter, O. *Nature (London)* **2009**, *459*, 550.
(9) Li, M.; Pernice, W.; Tang, H. *Nat. Nanotechnol.* **2009**, *4*, 377.
(10) Kang, M. S.; Nazarkin, A.; Brenn, A.; Russell, P. S. J. *Nat. Phys.* **2009**, *5*, 276.
(11) Teufel, J.; Donner, T.; Castellanos-Beltran, M.; Harlow, J.; Lehnert, K. *Nat. Nanotechnol.* **2009**, *4*, 820.
(12) Anetsberger, G.; Gavartin, E.; Arcizet, O.; Unterreithmeier, Q. P.; Weig, E. M.; Gorodetsky, M. L.; Kotthaus, J. P.; Kippenberg, T. J. *Phys. Rev. A* **2010**, *82*, 061804.
(13) Aspelmeyer, M.; Kippenberg, T. J.; Marquardt, F. *ArXiv* **2013**, arXiv:1303.0733 [cond-mat.mes-hall].
(14) Kippenberg, T. J.; Vahala, K. J. *Science* **2008**, *321*, 1172.
(15) Weeber, J.-C.; Bouhelier, A.; Colas des Francs, G.; Markey, L.; Dereux, A. *Nano Lett.* **2007**, *7*, 1352.
(16) Ou, J.-Y.; Plum, E.; Zhang, J.; Zheludev, N. I. *Nat. Nanotechnol.* **2013**, *8*, 252.
(17) Verbridge, S. S.; Parpia, J. M.; Reichenbach, R. B.; Bellan, L. M.; Craighead, H. *J. Appl. Phys.* **2006**, *99*, 124304.
(18) Halas, N. J.; Lal, S.; Chang, W.-S.; Link, S.; Nordlander, P. *Chem. Rev.* **2011**, *111*, 3913.
(19) Liu, N.; Hentschel, M.; Weiss, T.; Alivisatos, A. P.; Giessen, H. *Science* **2011**, *332*, 1407.
(20) Ding, L.; Baker, C.; Senellart, P.; Lemaitre, A.; Ducci, S.; Leo, G.; Favero, I. *Appl. Phys. Lett.* **2011**, *98*, 113108.
(21) Miljkovic, V. D.; Pakizeh, T.; Sepulveda, B.; Johansson, P.; Kall, M. *J. Phys. Chem. C* **2010**, *114*, 7472.
(22) Huang, C.; Zhu, L. *Opt. Lett.* **2010**, *35*, 1563.
(23) Woolf, D.; Loncar, M.; Capasso, F. *Opt. Express* **2009**, *17*, 19996.
(24) Anetsberger, G.; Arcizet, O.; Unterreithmeier, Q. P.; Riviére, R.; Schliesser, A.; Weig, E. M.; Kotthaus, J. P.; Kippenberg, T. J. *Nat. Phys.* **2009**, *5*, 909.
(25) Jensen, K.; Kim, K.; Zettl, A. *Nat. Nanotechnol.* **2008**, *3*, 533.
(26) Mamin, H. J.; Rugar, D. *Appl. Phys. Lett.* **2001**, *79*, 3358.
(27) Dionne, J.; Sweatlock, L.; Atwater, H.; Polman, A. *Phys. Rev. B* **2006**, *73*, 035407.
(28) Miyazaki, H. T.; Kurokawa, Y. *Phys. Rev. Lett.* **2006**, *96*, 097401.
(29) Hasan, S. B.; Filter, R.; Ahmed, A.; Vogelgesang, R.; Gordon, R.; Rockstuhl, C.; Lederer, F. *Phys. Rev. B* **2011**, *84*, 195405.
(30) Yu, P.-L.; Purdy, T. P.; Regal, C. A. *Phys. Rev. Lett.* **2012**, *108*, 083603.